Medicine®

DIAGNOSTIC ACCURACY STUDY

OPEN

Value of Dynamic Contrast-Enhanced MRI to Detect Local Tumor Recurrence in Primary Head and Neck Cancer Patients

Young Jun Choi, MD, Jeong Hyun Lee, MD, PhD, Yu Sub Sung, PhD, Ra Gyoung Yoon, MD, Ji Eun Park, MD, Soon Yuhl Nam, MD, PhD, and Jung Hwan Baek, MD, PhD

Abstract: Treatment failures in head and neck cancer patients are mainly related to locoregional tumor recurrence. The objective of the present study was to evaluate the diagnostic accuracy of model-free dynamic contrast-enhanced magnetic resonance imaging (DCE-MRI) to detect local recurrence during the surveillance of head and neck cancer patients.

Our retrospective study enrolled 24 patients with primary head and neck cancer who had undergone definitive treatment. Patients were grouped into local recurrence (n = 12) or posttreatment change (n = 12) groups according to the results of biopsy or clinicoradiologic follow-up. The types of time-signal intensity (TSI) curves were classified as follows: ''progressive increment'' as type I, ''plateau'' as type II, and ''washout'' as type III. TSI curve types and their parameters (i.e., wash-in, E_{max}, T_{max}, area under the curve [AUC]60, AUC90, and AUC120) were compared between the 2 study groups.

The distributions of TSI curve types for local recurrence versus posttreatment change were statistically significant ($P < 0.001$) (i.e., 0% vs 83.3% for type I, 58.3% vs 16.7% for type II, and 41.7% vs 0% for type III). There were statistically significant differences in E_{max}, T_{max}, and all of the AUC parameters between 2 groups ($P < 0.0083$ [0.05/6]). Receiver operating characteristic (ROC) curve analyses indicated that the TSI curve type was the best predictor of local recurrence with a sensitivity of 100% (95% CI, 73.5–100.0) and a specificity of 83.3% (95% CI, 51.6–97.9) (cutoff with type II).

Model-free DCE-MRI using TSI curves and TSI curve-derived parameters detects local recurrence in head and neck cancer patients with a high diagnostic accuracy.

(*Medicine* 95(19):e3698)

Abbreviations: AUC = area under the curve, DCE-MRI = dynamic contrast-enhanced magnetic resonance imaging, ROC = receiver operating characteristic, TSI = time-signal intensity.

Editor: Yong Liu.
Received: January 20, 2016; revised: April 12, 2016; accepted: April 23, 2016.
From the Department of Radiology and Research Institute of Radiology (YJC, JHL, YSS, RGY, JEP, JHB); and Department of Otolaryngology, University of Ulsan College of Medicine, Asan Medical Center, Seoul, Republic of Korea (SYN).
Correspondence: Jeong Hyun Lee, Department of Radiology and Research Institute of Radiology, University of Ulsan College of Medicine, Asan Medical Center, 86 Asanbyeongwon-Gil, Songpa-Gu, Seoul 138-736, Republic of Korea (e-mail: jeonghlee@amc.seoul.kr).
The authors have no funding and conflicts of interest to disclose.

ISSN: 0025-7974
DOI: 10.1097/MD.0000000000003698

INTRODUCTION

Treatment failure for head and neck cancer is mainly related to locoregional tumor recurrence (25%–54.9%), whereas distant metastasis occurs less frequently (2.3%–3.9%).[1–4] To increase the chances that a salvage procedure will be curative, posttreatment surveillance should aim to detect locoregional recurrent or persistent disease.[5] A definite diagnosis of locoregional tumor recurrence has been obtained through invasive procedures, such as biopsy or during surgery. The need for a biopsy itself can present a dilemma as the trauma of multiple biopsies in heavily radiated tissue may initiate superimposed infection, chondritis, failure to heal, further edema, and deterioration of complaints.[6] In addition, biopsies in previously treated areas may give false-negative results due to sampling errors associated with focally dispersed residual tumors. To supplement biopsy-related problems, diagnostic techniques should provide a better estimate of the likelihood of a recurrence and thus enable a more reliable selection of patients who should undergo a biopsy. Furthermore, a biopsy from recurrence might be of interest for the selection of next treatment option.

Conventional anatomical imaging techniques, such as computed tomography and magnetic resonance imaging (MRI), and advanced imaging techniques including diffusion-weighted MRI and fluorine-18 fluorodeoxyglucose positron emission tomography, have shown variable success in distinguishing posttreatment change from recurrent or persistent disease, with a good sensitivity (83%–100%) and specificity (74%–95%).[7–14] Dynamic contrast-enhanced magnetic resonance imaging (DCE-MRI) has proven to be accurate in the differentiation of recurrent or persistent disease and posttreatment change in regions such as the breast, pelvis, colon, and head and neck.[15–20] However, to the best of our knowledge, the value of the time-signal intensity (TSI) curve patterns and derived parameters from a model-free method for the assessment of treatment response for head and neck cancer has not been reported previously.

We hypothesized that the TSI curve and its associated parameters may differ between cases of recurrent or persistent disease, and between cases of posttreatment change on the basis of enhancement kinetics. Thus, the aim of this retrospective study was to evaluate the diagnostic accuracy of DCE-MRI using the TSI curve type and its derived parameters to predict locally recurrent tumor in the primary site during the follow-up of patients treated for head and neck cancer.

MATERIAL AND METHODS

Our retrospective study protocol was reviewed and approved by the institutional review board of our hospital. The requirement for written informed consent was waived due to the retrospective nature of the study. Our methods were

conducted in accordance with the Standards for Reporting Diagnostic Accuracy statement.[21]

Study Patients

The study population was obtained from a historical cohort of 97 consecutive patients who were diagnosed with head and neck cancer by pathology examination and undergone definite treatment including surgery, radiation therapy, or chemoradiation therapy at Asan Medical Center, a 2700-bed academic tertiary referral hospital in Seoul, Korea, between March, 2013 and July, 2014 (Figure 1). Of these, 52 patients had a radiologically measureable enhancing mass (>1 cm) or asymmetric soft-tissue thickening at primary site on posttreatment follow-up MRI including DCE-MRI.[22] Patients were excluded if they had any of the following criteria: poor image quality due to artifact or no final diagnosis (local recurrence or posttreatment change) either by histology or clinicoradiologic follow-up. Local recurrence was defined as histological (biopsy or surgery) confirmation of a tumor or an increase in the size of the mass. We defined increase in size as at least 20% increase in maximum diameter of enhancing lesion mass at the primary site on follow-up clinical or imaging examinations. Posttreatment change was defined as the absence of any new mass or increase in size of any preexisting enhancing lesion at the primary site during a follow-up period of at least 1 year or histological (biopsy or surgery) confirmation of posttreatment change. Finally, 24 patients were included in this study.

MR Techniques

DCE-MRI was performed using a 3-T MR scanner (Achieva; Philips Medical Systems, Best, The Netherlands) with a 16-channel neurovascular coil (SENSE NV coil; Philips Medical Systems). A 3-dimensional gradient echo data were obtained before, during, and after administration of a standard dose of 0.1 mmol of gadoterate meglumine (Dotarem; Guerbet, Paris, France) per kilogram of body weight at a rate of 4 mL/s with an MRI compatible power injector (Spectris; Medrad, Pittsburgh, PA). The bolus of contrast material was followed by a 25-mL bolus of saline, administered at the same injection rate. The dynamic acquisition was performed with a temporal resolution of 3.2 seconds by using the sensitivity encoding (SENSE) with SENSE factor 1.9 and partial Fourier sampling (0.8 for phase encoding direction; 0.8 for slice-select direction), and contrast was administrated after 14 baseline dynamics (total: 120 dynamics). The detailed imaging parameters for DCE-MRI were as follows: a slice thickness of 3 mm with no gap; 20 slices; z-axis coverage of 60 mm; spatial in-plane resolution of 184 × 160; TR/TE, 6.3/3.1 msec; flip angle, 15°; FOV, 19 cm; and total acquisition time of 6 minutes 24 seconds.

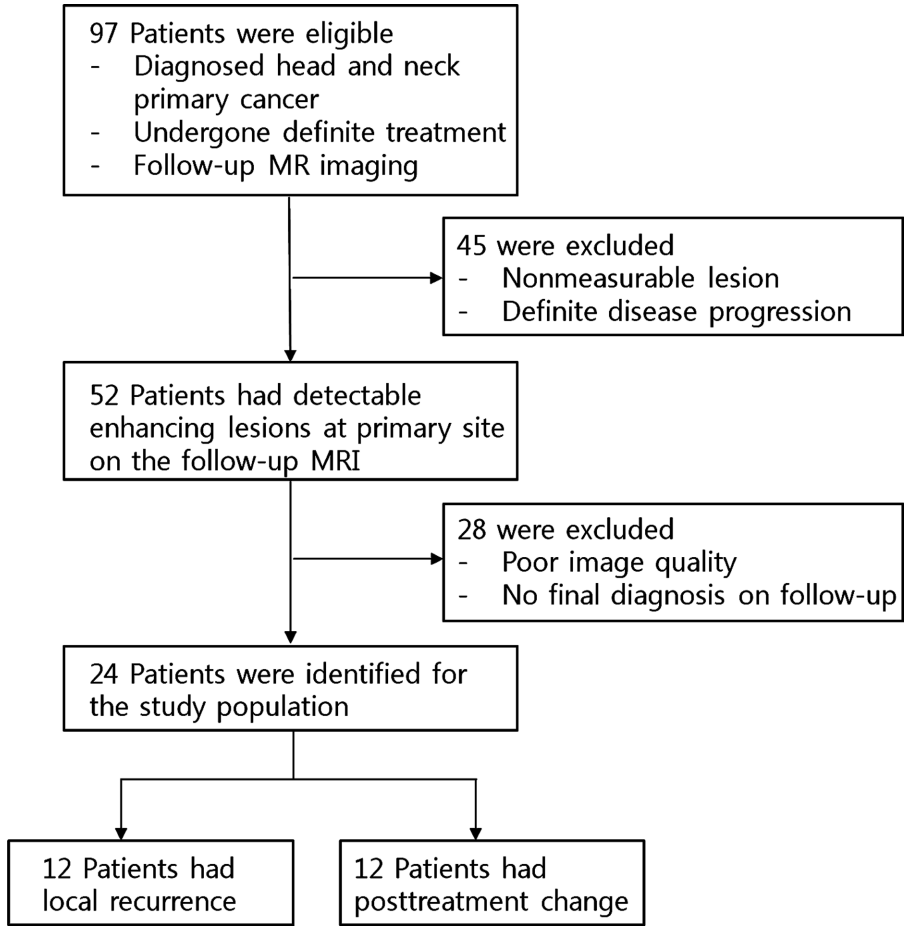

FIGURE 1. Patients flow diagram.

DCE-MRI was performed in an axial plane covering the entire tumor volume.

Image Processing and Analysis

MR data were digitally transferred from the picture archiving and communication system workstation to a personal computer and processed with the AFNI software (AFNI; http://afni.nimh.nih.gov/afni).[23] Regions of interest (ROIs) were drawn on all axial sections comprising any enhancing lesion present at the primary site, and then the volume of each enhancing lesion was generated by summing voxel volumes comprised within ROIs defined on all individual sections. We also measured the maximum axial diameter of each enhancing lesion. ROIs were drawn to avoid the major vessels and the cystic or necrotic part of the enhancing lesions as much as possible. The contrast index (CI) was calculated using the formula CI = [SI (postcontrast) − SI (precontrast)/SI (precontrast)].[24] The time course of the CI was then plotted to obtain a TSI curve. The TSI curve for each lesion was analyzed in 2 ways: subjective evaluation of the curve types and evaluation of its derived parameters. For the subjective evaluation, 2 experienced neuroradiologists (with 6 and 13 years of experience, respectively) independently performed a review of the TSI curves while blinded to the clinical and histopathologic findings and conventional MR images. Disagreement was resolved by consensus. Each curve was categorized according to the following classification: progressive increment (type I), plateau (type II), or washout of contrast agent (type III) (Figure 2). The following parameters were derived: E_{max}, T_{max}, wash-in, area under the curve (AUC)60, AUC90, and AUC120. The maximum CI (E_{max}) was considered to represent the maximum amplitude of enhancement, and T_{max} was defined as the time at which E_{max} occurred. Wash-in was defined as [CI (maximum) − CI (precontrast)/T_{max}]. The AUC60, AUC90, and AUC120 values were obtained by trapezoidal integration of the CI with time over 60, 90, and 120 seconds, respectively, after contrast agent arrival in the enhancing voxels of interest. This approach provides a measurement of the initial arrival of contrast agent in the tissue of interest after intravenous bolus administration that reflects blood flow, vascular permeability, and the fraction of interstitial space.[25]

Statistical Analysis

All statistical analyses were performed using MedCalc version 13.0 (MedCalc Software, Mariakierke, Belgium) for Windows. The significance threshold for differences was set at a P value of less than 0.05. To test the significance of individual subjective evaluations of TSI curve distribution in local recurrence and posttreatment change, we used the Chi-squared test. The Kolmogorov–Smirnov test was used to determine whether continuous variables of the TSI curve-derived parameters were normally distributed. According to the results of the Kolmogorov–Smirnov test, Student t test or the Mann–Whitney U test was performed for the comparison of 6 TSI curve-derived parameters between local recurrence and posttreatment change. The significance threshold for difference was set at a P value of less than 0.0083 (0.05/6) for multiple comparison correction. In the receiver operating characteristic (ROC) curve analysis, cutoff points of subjective evaluation and TSI curve-derived parameters determined by maximizing the sum of the sensitivity and specificity (Youden index = maximum sensitivity + maximum specificity − 1) were calculated to differentiate the 2 entities. In addition, the areas under the ROC curve of parameters and TSI curve types were compared using the method of DeLong et al.[26] A leave-one-out cross-validation was used to evaluate the performance of subjective evaluations of TSI curve type distributions. We calculated the interobserver agreement between subjective evaluations of TSI curve type distributions using kappa statistics.

RESULTS

A total of 24 patients were included in this study: clinical and radiologic follow-up examinations revealed local recurrence in 12 patients and posttreatment change in 12 patients in our current study series. For local recurrence, the final diagnosis was based on histopathological readings (n = 8, 66.7%) or increased mass on clinical and imaging follow-up (n = 4, 33.3%). For posttreatment change, the final diagnosis was based on histopathological readings (n = 3, 25.0%) or stable or decreased mass on clinical or imaging follow-up (n = 9, 75.0%) during a follow-up period of at least 1 year. Descriptive statistics regarding the demographic and clinical data obtained in both the local recurrence and posttreatment change are summarized in Table 1. Between local recurrence and posttreatment change groups, there were no statistically significant differences found in terms of age ($P = 0.778$), sex ($P = 0.193$), or the time interval ($P = 0.286$) between treatment end and DCE-MRI.

The shapes of the TSI curves differed significantly between patients with local recurrence and those with posttreatment change. In the local recurrence group, a type III curve was seen in 41.7% (5/12) of patients and a type II curve in 58.3% (7/12) of patients. In the posttreatment change group, the predominant TSI course was type I (83.3%; 10/12), a type II

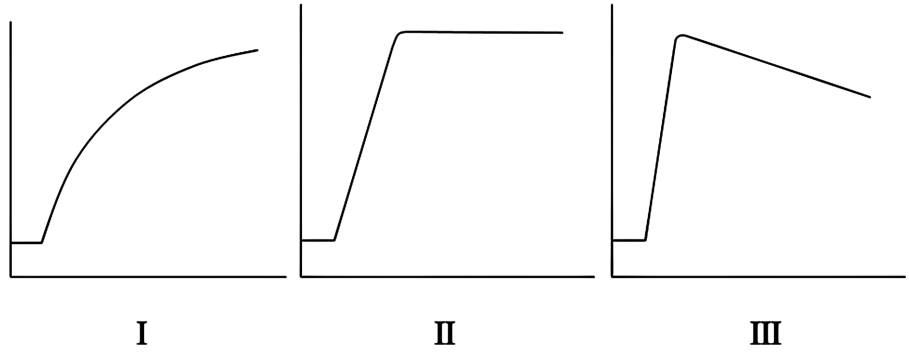

FIGURE 2. Type of time-signal intensity curve: type I, progressive increment; type II, plateau; and type III, washout.

TABLE 1. Demographic and Clinical Data for the Study Patients

No.	Age	Sex	Primary Site	Histologic Cell Type	Tx Modality	Time Interval, weeks	Final Diagnosis
1	55	F	Oral cavity	Squamous cell carcinoma	OP* + RTx	8.1	Local recurrence
2	46	M	Oral cavity	Squamous cell carcinoma	OP* + RTx	14.9	Local recurrence
3	38	M	Oral cavity	Squamous cell carcinoma	OP* + RTx	5	Local recurrence
4	39	M	Oral cavity	Squamous cell carcinoma	OP*	16.1	Local recurrence
5	49	M	Paranasal sinus	Squamous cell carcinoma	CCRT	8.3	Local recurrence
6	37	M	Paranasal sinus	Squamous cell carcinoma	OP*	27.1	Local recurrence
7	57	M	Paranasal sinus	Squamous cell carcinoma	CCRT	41.1	Local recurrence
8	29	F	Parotid gland	Mucoepidemoid carcinoma	OP*	87	Local recurrence
9	54	M	Parotid gland	Mucoepidemoid carcinoma	OP* + RTx	45.4	Local recurrence
10	61	M	Larynx	Squamous cell carcinoma	RTx	64.7	Local recurrence
11	60	M	Nasopharynx	Nonkeratinizing carcinoma	CCRT + OP†	44.3	Local recurrence
12	64	M	Oropharynx	Squamous cell carcinoma	RTx	30	Local recurrence
13	46	M	Paranasal sinus	Squamous cell carcinoma	CCRT	21.4	Posttreatment change
14	38	F	Paranasal sinus	Adenocarcinoma	CCRT	37.7	Posttreatment change
15	26	F	Paranasal sinus	Ewing's sarcoma	CCRT	198	Posttreatment change
16	62	F	Paranasal sinus	lymphoma	CCRT	11	Posttreatment change
17	68	M	Nasopharynx	Nonkeratinizing carcinoma	CCRT	50.4	Posttreatment change
18	60	F	Nasopharynx	Nonkeratinizing carcinoma	CCRT	158.4	Posttreatment change
19	60	M	Nasopharynx	Nonkeratinizing carcinoma	CCRT	3.1	Posttreatment change
20	43	M	Nasopharynx	Nonkeratinizing carcinoma	CCRT	8.9	Posttreatment change
21	49	M	Nasopharynx	Nonkeratinizing carcinoma	CCRT	129.9	Posttreatment change
22	34	F	Oral cavity	Squamous cell carcinoma	OP*	3	Posttreatment change
23	48	F	Orbit	Lymphoma	CCRT	15.1	Posttreatment change
24	73	M	External auditory canal	Squamous cell carcinoma	OP* + RTx	27.3	Posttreatment change

CCRT = concurrent chemoradiation therapy, CTx = chemotherapy, OP = operation, MRI = magnetic resonance imaging, RTx = radiation therapy.
*Surgery for primary tumor site with microscopic tumor clearance.
†Surgery for neck lymph node with microscopic tumor clearance. Time interval is the period between treatment end and model-free dynamic contrast-enhanced MRI.

curve was identified in 16.7% (2/12) of patients, but no type III curve was found in any patient. The Chi-squared test demonstrated a statistically significant difference in the distribution of the curve types in the local recurrence and posttreatment change groups ($P < 0.001$). If types II and III were used as a criteria to diagnose local recurrence, and a type I curve was considered suggestive of posttreatment change, the following diagnostic indices for the type of the TSI curve criterion emerged: area under the curve (Az), 0.951 (95% CI, 0.779–0.998); sensitivity, 100% (95% CI, 73.5–100.0); specificity, 83.3% (95% CI, 51.6–97.9); positive predictive value, 85.7%; negative predictive value, 100%; and diagnostic accuracy, 91.7%, when all were regarded as a training set. Leave-one-out cross-validation tests for the type of the TSI curve revealed same diagnostic accuracy, sensitivity, and specificity. The likelihood of local recurrence associated with a type I, II, or III TSI curve was 0% (0/10), 77.8% (7/9), and 100% (5/5), respectively. A false-positive result was found in 2 of 11 patients with posttreatment change (patient no. 19 and 22), for whom the histology of the primary head and neck cancer were nasopharyngeal nonkeratinizing carcinoma and oral tongue squamous cell carcinoma, respectively. These lesions were also false-positive on TSI curve-derived parameter analysis (i.e., AUC60 value, see below).

The 2 readers came to concordant results for TSI curve classification in 21 (87.5%) of the 24 cases we analyzed. In 3 cases (12.5%) with a discordant rating, type II of 2 cases and type I of 1 case were selected by consensus. The kappa value was 0.839 (95% CI, 0.671–1.000), indicating almost perfect agreement ($P < 0.001$).

The TSI curve-derived parameters between the local recurrence and posttreatment change groups in our study are summarized in Table 2. The mean values of the E_{max}, AUC60, AUC90, and AUC120 were significantly higher in the local recurrence group than in the posttreatment change group. In addition, the mean T_{max} was significantly longer in the posttreatment change patients. We subsequently performed ROC curve analysis of the mean E_{max}, T_{max}, AUC60, AUC90, and AUC120 values between the local recurrence and posttreatment change groups. The mean AUC60 was found to be the single best predictive TSI curve-derived parameter with an estimated cut-off of 50.08 because the Az was highest among the parameters without statistical difference ($P > 0.1$). The following diagnostic indices for the mean AUC60 emerged: Az, 0.882 (95% CI, 0.685–0.977); sensitivity, 91.7% (95% CI, 61.5–99.8); and specificity, 83.3% (95% CI, 51.6–97.9). Representative cases are detailed in Figures 3 and 4. The Az for the type of the TSI curve was higher compared with the single best predictive parameter (AUC60) without statistical difference (0.951 vs 0.882, respectively; $P = 0.287$) (Figure 5).

DISCUSSION

The results of our present study can be summarized as follows. First, enhancement kinetics, as represented by the type

TABLE 2. Difference in the Size and TSI Curve-Derived Parameters of Model-Free DCE-MRI Between the Local Recurrence and Posttreatment Change Groups

Parameters	Local Recurrence	Posttreatment Change	*P* Value
Tumor diameter, cm	3.8 ± 1.0	3.4 ± 0.9	0.192
ROI lesion volume, cm^3	37.1 ± 29.6	24.6 ± 34.8	0.351
Wash-in	0.09 ± 0.10	0.03 ± 0.02	0.040
E_{max}	2.44 ± 0.91	1.60 ± 0.40	0.008
T_{max}, second	59.58 ± 28.00	104.22 ± 35.54	0.008
AUC60	94.58 ± 42.13	45.43 ± 18.98	0.001
AUC90	152.21 ± 64.39	75.69 ± 30.85	0.001
AUC120	212.02 ± 86.87	108.14 ± 42.38	0.001

Data are the mean ± standard deviations. *P* values were calculated using Student *t* test because all parameters passed normality test (the Kolmogorov–Smirnov test). For definitions of the indicated parameters, please see the Image Processing and Analysis section of the Materials and Methods. AUC = area under the curve, DCE-MRI = dynamic contrast-enhanced magnetic resonance imaging, ROI = region of interest, TSI = time-signal intensity.

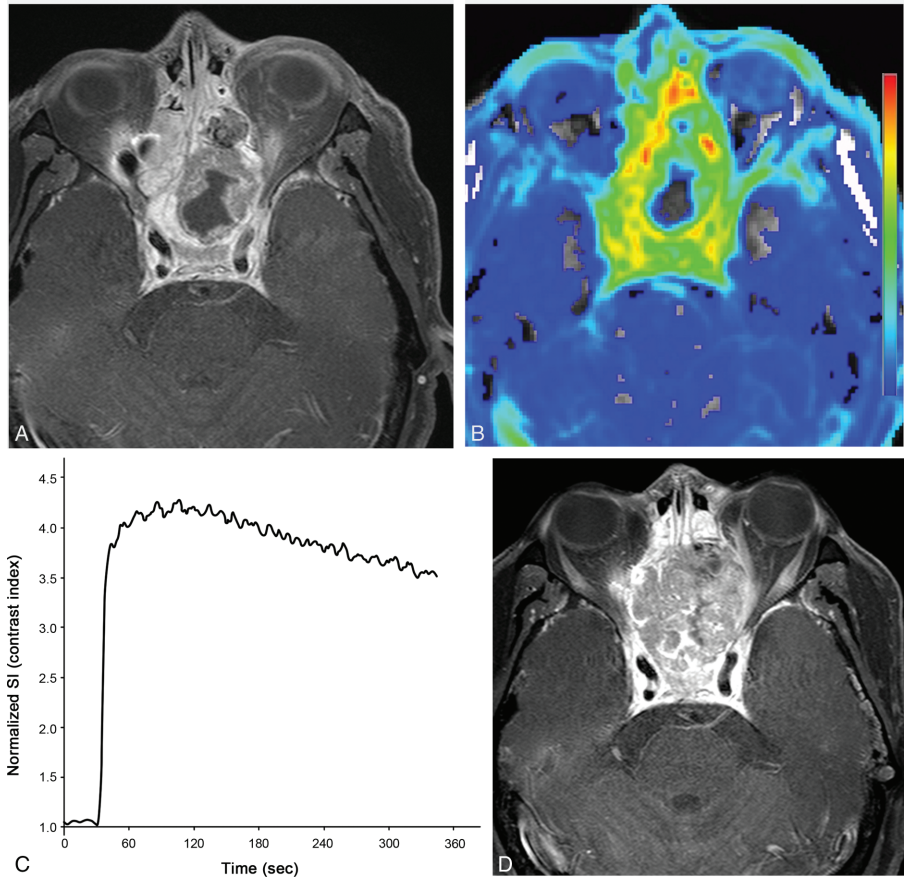

FIGURE 3. Local recurrence of a nasopharyngeal cancer in a 60-year-old man. (A) Contrast-enhanced T1-weighted MRI showing an expansile mass in the ethmoidal and sphenoidal sinuses after treatment. (B) AUC60 map derived from DCE-MRI analysis showing a relatively fast visual increase in AUC in the corresponding areas of the contrast-enhancing lesion. (C) TSI curve of the entire enhancing lesion showing wash-out (type III) with an AUC60 value of 154.03. (D) 26-week follow-up MRI showing an increase in mass size, thus suggesting local recurrence. AUC = area under the curve, DCE-MRI = dynamic contrast-enhanced magnetic resonance imaging, MRI = magnetic resonance imaging, TSI = time-signal intensity.

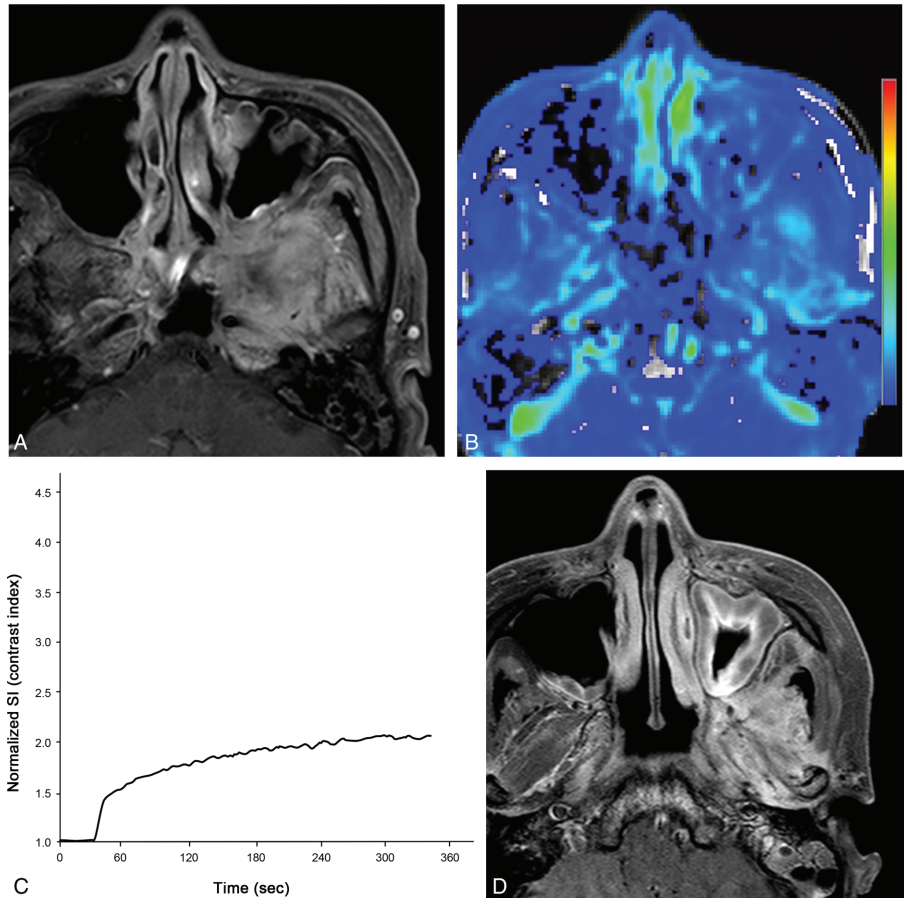

FIGURE 4. Posttreatment change of maxillary sinus cancer in a 38-year-old woman. (A) Contrast-enhanced T1-weighted MRI showing a retracted mass with enhancement in the infratemporal fossa after treatment. (B) AUC60 map derived from DCE-MRI analysis showing a relatively slow visual increase in AUC in the corresponding areas of the contrast-enhancing lesion. (C) TSI curve of the entire enhancing lesion showing a progressive increment (type I), and an AUC60 value of 28.49. (D) 82-week follow-up MRI showing a reduction in mass size, thus suggesting posttreatment change. AUC = area under the curve, DCE-MRI = dynamic contrast-enhanced magnetic resonance imaging, MRI = magnetic resonance imaging, TSI = time-signal intensity.

of TSI curve, were significantly different between the local recurrence and posttreatment change patients in our study series after treatment for head and neck cancer. In the local recurrence group, plateau or wash-out (type II or III) TSI curves prevailed. In contrast, the posttreatment change group predominantly exhibited progressive increment (type I) TSI curves. Second, multiple TSI curve-derived parameters were significantly different between local recurrence and posttreatment change patients. These findings can be explained as follows. Local recurrence, that is, recurrent or residual tumor, shows early and intense enhancement because of its hypervascularity, leaky vessels, and high cellularity. In contrast, posttreatment changes, such as a scar, show persistent delayed enhancement by virtue of the greater contrast agent retention in the extravascular extracellular space due to fibrosis and tissue damage.[27–29]

DCE-MRI has been used to differentiate recurrence from posttreatment change of cancer in the head and neck as well as in other organs such as the breast, colon, and cervix. And they have revealed that DCE-MRI demonstrates different enhancement patterns for enhancing suspicious lesions after bolus injection of gadolinium contrast agent; early enhancement corresponded to recurrence, while weakly enhanced areas corresponded to fibrotic scarring and necrosed lesions.[15–20] Our current results are very similar to these previous results, emphasizing the potential value of DCE-MRI in differentiating recurrence from posttreatment change in head and neck.

It is notable that 2 of our 12 present study patients who had posttreatment change were misclassified as local recurrence cases in the subjective evaluation of TSI curve analysis. We speculate that the interval between the end of treatment and MRI, rather than primary tumor histologic cell type, may be an important factor in our current study population. DCE-MRI was performed just 3 weeks after treatment in these 2 false-positive cases of posttreatment change, which may indicate that post-treatment inflammation and edema were still present. Previous studies have demonstrated that a short time interval between treatment and MRI may result in false-positives on DCE-MRI[18] and that edema and acute or chronic inflammation could lead to false-positives on MRI in the first 3 to 4 months after treatment.[30]

Comparing model-based and model-free DCE-MRI parameters, Roberts et al[31] concluded that although modeling is more complex than the model-free approach, the former is preferable as it provides greater physiologic insight. In contrast,

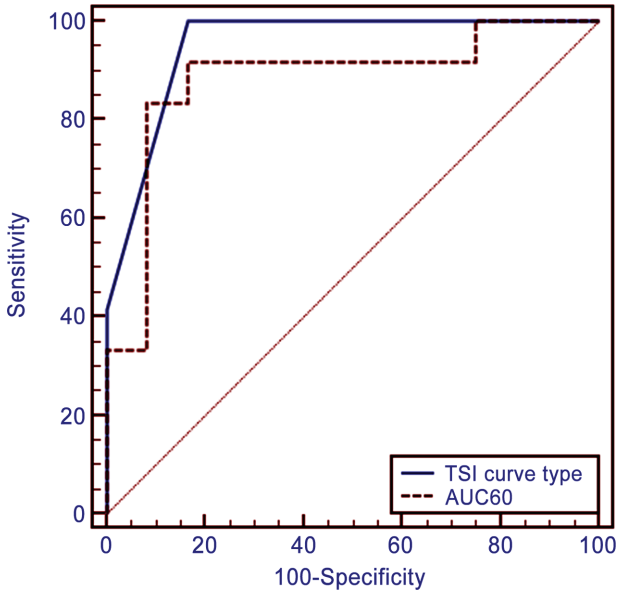

FIGURE 5. Comparison of ROC curves of the TSI curve type and AUC60 differentiating local recurrence and posttreatment change. The area under the curve of the TSI curve type was 0.951 (95% CI, 0.779–998) and AUC60 was 0.882 (95% CI, 0.685–0.977). For definitions of the indicated parameters, please see the Image Processing and Analysis section of the Materials and Methods. AUC = area under the curve, CI = confidence interval, ROC = receiver operating characteristic, TSI = time-signal intensity.

Evelhoch[32] suggested that AUC is related to blood flow, vessel permeability, and the fraction of interstitial space. The model-free DCE-MRI parameters, including AUC parameters, are generally preferred for several reasons: temporal resolution requirements are relaxed because an arterial input function measurement is not needed, and the potential for fit failure owing to signal noise is irrelevant because data fitting is not required. In addition, model-free systems are more robust and practical because TSI curve fitting and extraction of parameters from the curves are easier and more reproducible than in the model-based method.[33–35] Hence, we here adopted a model-free method and validated the value of TSI curve- and AUC-derived DCE-MRI parameters. However, further studies should be necessary to compare model-free and model-based methods for further validation.

Our study has several limitations of note. First, it was a retrospective discovery-phase study with a small group of patients with heterogeneous histologic subtypes and various treatment protocols. However, our DCE-MRI study demonstrated coherent results irrespective of the heterogeneous histologic subtypes and various treatment protocols. This could be explained by the fact that histologic end results after surgery or cytotoxic therapies are variable degree of tissue damage, granulation tissue, and fibrosis in contrast to hypervascularity, leaky vessels, and high cellularity of malignant tumors. Further prospective studies that include a larger population are needed to validate our study result and the usefulness of DCE-MRI in patients according to different histologic types of malignancy. Second, we did not compare conventional MRI with DCE-MRI. Although DCE-MRI itself showed high diagnostic accuracy by the analysis of TSI curve patterns or TSI curve-derived parameters, the context in which DCE-MRI provides additional diagnostic value to conventional MRI findings remains unknown. However, we believe that this preliminary study on posttreatment head and neck cancer provides important background data for future evaluations of the added value of DCE-MRI in larger populations.

In conclusion, our current clinical investigation shows that model-free DCE-MRI using TSI curves and TSI curve-derived parameters is feasible and reproducible for detecting local tumor recurrence during follow-up of head and neck cancer patients, with Az values ranging from 0.779 to 0.998. These results may be used as a fundamental basis for designing further studies with larger patient populations to assess the added value of DCE-MRI for evaluating head and neck cancer patients.

ACKNOWLEDGEMENTS

The authors thank the technical support of Hye-jung Ju and A Ra Choi from Biomedical Imaging Infrastructure, Department of Radiology, Asan Medical Center.

REFERENCES

1. Gonçalves Agra IM, Lopes Carvalho A, Samsonovski Ulbrich F, et al. Prognostic factors in salvage surgery for recurrent oral and oropharyngeal cancer. *Head Neck.* 2006;28:107–113.
2. Carvalho AL, Magrin J, Kowalski LP. Sites of recurrence in oral and oropharyngeal cancers according to the treatment approach. *Oral Dis.* 2003;9:112–118.
3. Goodwin WJ Jr. Salvage surgery for patients with recurrent squamous cell carcinoma of the upper aerodigestive tract: when do the ends justify the means? *Laryngoscope.* 2000;110(3 Pt 2 Suppl 93):1–18.
4. Kowalski LP, Bagietto R, Lara JR, et al. Prognostic significance of the distribution of neck node metastasis from oral carcinoma. *Head Neck.* 2000;22:207–214.
5. Yom SS, Machtay M, Biel MA, et al. Survival impact of planned restaging and early surgical salvage following definitive chemoradiation for locally advanced squamous cell carcinomas of the oropharynx and hypopharynx. *Am J Clin Oncol.* 2005;28:385–392.
6. Bahadur S, Amatya R, Kacker S. The enigma of post-radiation oedema and residual or recurrent carcinoma of the larynx and pyriform fossa. *J Laryngol Otol.* 1985;99:763–765.
7. Kim S, Loevner L, Quon H, et al. Diffusion-weighted magnetic resonance imaging for predicting and detecting early response to chemoradiation therapy of squamous cell carcinomas of the head and neck. *Clin Cancer Res.* 2009;15:986–994.
8. Vandecaveye V, De Keyzer F, Nuyts S, et al. Detection of head and neck squamous cell carcinoma with diffusion weighted MRI after (chemo) radiotherapy: correlation between radiologic and histopathologic findings. *Int J Radiat Oncol Biol Phys.* 2007;67:960–971.
9. Abgral R, Querellou S, Potard G, et al. Does 18F-FDG PET/CT improve the detection of posttreatment recurrence of head and neck squamous cell carcinoma in patients negative for disease on clinical follow-up? *J Nucl Med.* 2009;50:24–29.
10. Ong SC, Schöder H, Lee NY, et al. Clinical utility of 18F-FDG PET/CT in assessing the neck after concurrent chemoradiotherapy for locoregional advanced head and neck cancer. *J Nucl Med.* 2008;49:532–540.
11. King AD, Keung CK, Yu KH, et al. T2-weighted MR imaging early after chemoradiotherapy to evaluate treatment response in head and neck squamous cell carcinoma. *Am J Neuroradiol.* 2013;34:1237–1241.

12. Hermans R, Pameijer FA, Mancuso AA, et al. Laryngeal or hypopharyngeal squamous cell carcinoma: can follow-up CT after definitive radiation therapy be used to detect local failure earlier than clinical examination alone? *Radiology.* 2000;214:683–687.
13. de Bree R, van der Putten L, Brouwer J, et al. Detection of locoregional recurrent head and neck cancer after (chemo) radiotherapy using modern imaging. *Oral Oncol.* 2009;45:386–393.
14. Ojiri H, Mendenhall WM, Mancuso AA. CT findings at the primary site of oropharyngeal squamous cell carcinoma within 6-8 weeks after definitive radiotherapy as predictors of primary site control. *Int J Radiat Oncol Biol Phys.* 2002;52:748–754.
15. Dao TH, Rahmouni A, Campana F, et al. Tumor recurrence versus fibrosis in the irradiated breast: differentiation with dynamic gadolinium-enhanced MR imaging. *Radiology.* 1993;187:751–755.
16. Kerslake R, Fox J, Carleton P, et al. Dynamic contrast-enhanced and fat suppressed magnetic resonance imaging in suspected recurrent carcinoma of the breast: preliminary experience. *Br J Radiol.* 1994;67:1158–1168.
17. Hawighorst H, Knapstein PG, Schaeffer U, et al. Pelvic lesions in patients with treated cervical carcinoma: efficacy of pharmacokinetic analysis of dynamic MR images in distinguishing recurrent tumors from benign conditions. *Am J Roentgenol.* 1996;166:401–408.
18. Kinkel K, Tardivon AA, Soyer P, et al. Dynamic contrast-enhanced subtraction versus T2-weighted spin-echo MR imaging in the follow-up of colorectal neoplasm: a prospective study of 41 patients. *Radiology.* 1996;200:453–458.
19. Kinkel K, Ariche M, Tardivon AA, et al. Differentiation between recurrent tumor and benign conditions after treatment of gynecologic pelvic carcinoma: value of dynamic contrast-enhanced subtraction MR imaging. *Radiology.* 1997;204:55–63.
20. Semiz Oysu A, Ayanoglu E, Kodalli N, et al. Dynamic contrast-enhanced MRI in the differentiation of posttreatment fibrosis from recurrent carcinoma of the head and neck. *Clin Imaging.* 2005;29:307–312.
21. Bossuyt PM, Reitsma JB, Bruns DE, et al. STARD 2015: an updated list of essential items for reporting diagnostic accuracy studies. *BMJ (Clin Res Ed).* 2015;351:h5527.
22. Eisenhauer E, Therasse P, Bogaerts J, et al. New response evaluation criteria in solid tumours: revised RECIST guideline (version 1.1). *Eur J Cancer.* 2009;45:228–247.
23. Cox RW. AFNI: software for analysis and visualization of functional magnetic resonance neuroimages. *Comput Biomed Res.* 1996;29:162–173.
24. Matsuzaki H, Yanagi Y, Hara M, et al. Minor salivary gland tumors in the oral cavity: diagnostic value of dynamic contrast-enhanced MRI. *Eur J Radiol.* 2012;81:2684–2691.
25. Evelhoch JL, LoRusso PM, He Z, et al. Magnetic resonance imaging measurements of the response of murine and human tumors to the vascular-targeting agent ZD6126. *Clin Cancer Res.* 2004;10:3650–3657.
26. DeLong ER, DeLong DM, Clarke-Pearson DL. Comparing the areas under two or more correlated receiver operating characteristic curves: a nonparametric approach. *Biometrics.* 1988:837–845.
27. Padhani AR. Dynamic contrast-enhanced MRI in clinical oncology: current status and future directions. *J Magn Reson Imaging.* 2002;16:407–422.
28. Padhani AR, Husband JE. Dynamic contrast-enhanced MRI studies in oncology with an emphasis on quantification, validation and human studies. *Clin Radiol.* 2001;56:607–620.
29. Narang J, Jain R, Arbab AS, et al. Differentiating treatment-induced necrosis from recurrent/progressive brain tumor using nonmodel-based semiquantitative indices derived from dynamic contrast-enhanced T1-weighted MR perfusion. *Neuro Oncol.* 2011;13:1037–1046.
30. Lell M, Baum U, Greess H, et al. Head and neck tumors: imaging recurrent tumor and post-therapeutic changes with CT and MRI. *Eur J Radiol.* 2000;33:239–247.
31. Roberts C, Issa B, Stone A, et al. Comparative study into the robustness of compartmental modeling and model-free analysis in DCE-MRI studies. *J Magn Reson Imaging.* 2006;23:554–563.
32. Evelhoch JL. Key factors in the acquisition of contrast kinetic data for oncology. *J Magn Reson Imaging.* 1999;10:254–259.
33. Chung WJ, Kim HS, Kim N, et al. Recurrent glioblastoma: optimum area under the curve method derived from dynamic contrast-enhanced T1-weighted perfusion MR imaging. *Radiology.* 2013;269:561–568.
34. Galbraith SM, Lodge MA, Taylor NJ, et al. Reproducibility of dynamic contrast-enhanced MRI in human muscle and tumours: comparison of quantitative and semi-quantitative analysis. *NMR Biomed.* 2002;15:132–142.
35. Hamilton JD, Lin J, Ison C, et al. Dynamic contrast-enhanced perfusion processing for neuroradiologists: model-dependent analysis may not be necessary for determining recurrent high-grade glioma versus treatment effect. *AJNR Am J Neuroradiol.* 2015;36:686–693.